# Methanation of carbon dioxide on $Ru/Al_2O_3$ and $Ni/Al_2O_3$ catalysts at atmospheric pressure: catalysts activation, behaviour and stability

Gabriella Garbarino[1], Daria Bellotti[2], Paola Riani[3], Loredana Magistri[2], Guido Busca[1]*

1 Università degli Studi di Genova, Dipartimento di Ingegneria Civile, Chimica e Ambientale (DICCA), P.zzale Kennedy, 1 16129 Genova, Italy

2 Università degli Studi di Genova, Dipartimento di Ingegneria Meccanica, Energetica, Gestionale e dei Trasporti (DIME), Via all'Opera Pia, 15 16145 Genova, Italy

3 Università degli Studi di Genova, Dipartimento di Chimica e Chimica Industriale (DCCI), Via Dodecaneso, 31 16146 Genova, Italy

* e-mail: Guido.Busca@unige.it; phone +390103536024; fax +390103536028.

Abstract. The methanation of carbon dioxide has been studied over a 3% $Ru/Al_2O_3$ and a 20% $Ni/Al_2O_3$ commercial catalysts. Experiments have been performed in diluted conditions in a flow catalytic reactor with a continuous IR detection of products. The data reported here confirm that 3% $Ru/Al_2O_3$ is an excellent catalyst for $CO_2$ methanation (96 % methane yield with no CO coproduction at 573 K at 30000 $h^{-1}$ GHSV in excess hydrogen). The performance is better than that of $Ni/Al_2O_3$ catalyst. The reaction orders over both catalysts with respect to both hydrogen and $CO_2$ were determined over conditioned catalysts. An on stream conditioning of the $Ru/Al_2O_3$ catalyst was found to be needed and more effective than conditioning in hydrogen, associated to cleaning of the surface from chlorine impurities, occurring in-situ during methanation reaction possibly as an effect of huge water formation. The conditioned $Ru/Al_2O_3$ catalyst was found to retain stable high activity after different shut-down and start-up procedures, thus being possibly applicable in intermittent conditions.

Keywords: Hydrogen; carbon dioxide; methanation; ruthenium on alumina; activation of the catalyst; stability.

## 1.Introduction.

The hydrogenation of $CO_2$ with renewable hydrogen is an interesting option as a $CO_2$ Capture and Storage technology (CCS) to reduce the emissions of greenhouse gases, with producing useful compounds. Although a number of different compounds could in principle be formed by $CO_2$ hydrogenations (e.g. all hydrocarbons, alcohols, formic acid, etc.), the production of methane (methanation)

$CO_2 + 4\ H_2 \rightarrow\ CH_4 + \ 2H_2O$ $\quad \Delta H°_{298}\ = -165.12$ kJ/mol (1)

could allow to reuse carbon atoms as an energy vector. This reaction is presumed to be strictly related to the CO methanation reaction

$CO + 3\ H_2 \rightarrow\ CH_4 + \ H_2O$ $\quad \Delta H°_{298} = -\ 206.28$ kJ/mol (2)

CO being possibly an intermediate in $CO_2$ methanation, arising from the so called reverse water gas shift reaction,

$CO_2 + H_2 \rightarrow\ CO + H_2O$ $\quad \Delta H°_{298} = +\ 41.16$ kJ/mol (3)

The methanation of CO, usually in the presence of small amounts of $CO_2$, is applied industrially since decades to reduce residual carbon oxides present in hydrogen for ammonia synthesis [1,2]. For this application commercial catalysts are based on $Ni/Al_2O_3$ [3,4,5], with quite a high surface area for the alumina support (100-250 $m^2/g$) [6]. A catalyst offered by Clariant for standard application (METH-134) is reported to contain 25% NiO on alumina [5] while catalysts with a higher Ni-content are reported to provide a higher activity at low-temperature and to be suitable for higher space velocities. A catalyst for low temperature application (463 K-723 K) offered by Topsøe (PK-7R) [7] is reported to contain 20-25 % Ni (w/w) [8]. For extremely low temperature applications (T < 443 K) Clariant offers a catalyst (METH-150) containing 0.3 % ruthenium on alumina [5].

In a different process, CO-rich gas methanation is performed to produce Substitute Natural Gas (SNG). Due to the exothermicity of the reaction and the high concentration of $CO_x$ in this case, the catalyst bed temperature is actually varying in larger ranges (up to 973 K) [9,10]. The high temperature methanation catalyst Topsøe MCR is reported to have stable activity up to 973 K [11]. Publications report about the use of a 22% Ni catalyst on a stabilized support, with a surface area decreasing from 50 $m^2/g$ (fresh) to 30 $m^2/g$ (used) [12].

Conventional methanation catalysts have been optimized to convert feeds containing primarily carbon monoxide. To date, commercial catalysts optimized for methanation feeds primarily composed of carbon dioxide are apparently lacking.

A number of studies are currently undertaken to characterize $CO_2$ hydrogenation processes and to develop and optimize catalysts [13]. While catalysts based on $Ni/Al_2O_3$ are confirmed to be very active also in $CO_2$ methanation [14,15], the coproduction of CO depends on catalyst loading and pretreatment. In a recent patent application, the preparation of a coprecipitated Ni-Cr catalyst, as such or in the presence of silica, is described. The Ni:Cr ratio can vary from 98:2 to 50:50 [16]. Rhodium based catalysts were reported to be effective for $CO_2$ hydrogenation giving 100% selectivity to methane at 478-523 K [17]. A number of studies also show good performances of $Ru/Al_2O_3$ catalysts [18,19]. One of the points to be taken into account, depending on the practical application of $CO_2$ methanation, concerns the activation needed to obtain optimal activity, taking into account that in most cases intermittent operations may be considered.

In this paper we report our data of a study on the catalytic activity of a commercial 3% $Ru/Al_2O_3$ catalyst and on its activation and stability. The behavior of this catalyst will also be compared with that of a commercial $Ni/Al_2O_3$ catalyst.

## 2. Experimental

### *2.1 Materials preparation*

The catalyst used in this study is a 3% $Ru/Al_2O_3$ commercial catalyst from Acta S.p.A. (Crespina, Pisa, Italy). Some experiments are reported using a 20% $Ni/Al_2O_3$ catalyst from the same source. Surface area measurement were done with a single point BET method after previous outgassing at 573 K in vacuum. X-ray diffraction patterns were carried out by using a vertical powder diffractometer X'Pert with Cu $K_\alpha$ radiation ($\lambda$ = 0.15406 nm). The patterns were collected in the 25 – 100° 2$\theta$ range with a step of 0.03° and a counting time for each step of 12 s. Powder patterns were indexed by comparing experimental results to the data reported in the Pearson's Crystal Data database [20].

Micrographs of both fresh and spent samples were collected with a SEM ZEISS SUPRA 40 VP microscope, equipped with a field emission gun, a high sensitivity "InLens" secondary electron detector and with a EDX microanalysis OXFORD "INCA Energie 450x3". Samples for SEM analysis were suspended in ethanol under ultrasonic vibrations to decrease particle aggregation. A drop of the resultant mixture was finally deposed on a Lacey Carbon copper grid.

*2.2 Catalytic experiments.*

Catalytic experiments were carried out in a fixed-bed tubular silica glass flow reactor, operating isothermally, loaded with 700 mg of silica glass particles (60-70 mesh sieved) as an inert material mixed with variable amounts of catalyst powder. Gaseous mixtures of $CO_2$ and $H_2$ (with excess $H_2$) diluted with nitrogen were fed, 75 $ml_{NTP}$/min. Temperature was varied step by step in-between 523 K and 773 K and back down to 523 K. GHSV was varied in between 15000 and 55000 $h^{-1}$. Experiments have been performed without any pretreatment ("as received sample") or after a prereduction. In some cases for $Ru/Al_2O_3$ catalyst in-situ prereduction was performed by flowing a 20% $H_2/N_2$ mixture (vol/vol) at 673 K for 30 minutes and then keeping in $N_2$ until room temperature was reached ("prereduced sample"). Both families of catalysts have also been characterized after reaction ("spent samples" and "prereduced spent samples").

Products analysis was performed on line using a Nicolet 6700 FT-IR instrument with previous calibration using gas mixtures with known concentrations, in order to have quantitative results. Produced water was partially condensed before the IR cell.

$CO_2$ conversion ($X_{CO2}$), selectivities and yields to products, $S_i$ and $Y_i$, are defined as:

$$X_{CO2} = \frac{n_{CO2\ in} - n_{CO2\ out}}{n_{CO2\ in}} \quad (4);$$

$$S_i = \frac{n_i}{n_{CO2\ in} - n_{CO2\ out}} \quad (5);$$

$$Y_i = \frac{n_i}{n_{CO2\ in}} \quad (6);$$

In order to investigate kinetic aspects the catalysts was pretreated in the reactant mixture at 648 K. To study the $CO_2$ reaction order, $CO_2$ partial pressure was varied in-between 0.02 atm and 0.07 atm while maintaining constant $pH_2$ (0.30 atm) at 493 K and 523 K for Ruthenium and Nickel based catalysts respectively, in which the hypothesis of a differential reactor can be applied. The same procedure was done to study the reaction order with respect $H_2$ concentration, where $p_{H2}$ was varied from 0.03 atm to 0.21 atm at constant $p_{CO2}$ (0.07 atm). At low temperature an extimation of $CO_2$ methanation activation energy was done, using the conversions values obtained under kinetic control at 493 K, 523 K and 573 K, using Arrhenius plots in a differential reactor hypothesis [21].

## 3. Results and discussion.

Measured surface areas are 150 $m^2/g$ for $Ru/Al_2O_3$ and 132 $m^2/g$ for $Ni/Al_2O_3$. XRD analyses confirmed that both catalysts are supported on a $\gamma$-alumina. No evidence of ruthenium metal or oxide phases was obtained for $Ru/Al_2O_3$ while for $Ni/Al_2O_3$ XRD pattern shows the presence of cubic metallic Ni. Both catalysts are black. DR-UV-vis-NIR spectra show a strong continuous absorption for both catalysts suggesting that the metal elements are largely in the metallic state in both cases.

In Fig. 1, the results of a typical experiment on $Ru/Al_2O_3$ catalyst are reported. In this case 82.2 mg of the as received catalyst has been put in the reactor, the feed composition was set at $CO_2$ 6 %, $H_2$ 30 % and $N_2$ 64 % with a total flow of 75 Nml/min. Thus, the GHSV was 55000 $h^{-1}$. Preliminarily, calibration curves showed in all cases that the absorbance/concentration relations deviate slightly from linearity. Products concentrations have been calculated from the absorbances recorded, as in the figure, using the calibration curves.

In the experiment in Fig.1 the temperature was raised step by step of 50 K every 25 minutes. From Fig. 1 it is evident that the fresh catalyst is almost not active at 523 K and is only very slightly active at 573 K, with a small methane yield slightly increasing with time on stream. In the step at 623 K the catalyst starts to have significant activity, that definitely increases with time on stream. In these conditions selectivity to methane is 100 %, being neither CO nor any other compound detected. At 673 K, $CO_2$ conversion is high but still growing with time on stream, showing that a “conditioning” effect was still in progress. At this temperature some CO is also formed together with methane. No other compounds are detected. During the step at 723 K, instead, the conversion is almost stable, suggesting that the catalyst has been converted into a fully active form. At the maximum temperature investigated here, $CO_2$ conversion is slightly decreased. Thermodynamic calculations [22], whose results are summarized in Table 1, reveal that in our conditions we come near to thermodynamic equilibrium at 773 K and 723 K, that implies a decrease of $CO_2$ conversion by increasing temperature. In agreement with this, the $CO_2$ conversion and methane yield decrease at 773 K, and re-increase in the further decreasing temperature steps at 723 K and 673 K. We can note that the $CO_2$ conversion and $CH_4$ yield observed at 673 K in the decreasing temperature step are higher than those observed, at the same temperature, in the increasing temperature experiment. This confirms the “conditioning” of the catalyst in

the previous steps at 623-723 K. We can mention that in the step at 673 K still the $CO_2$ and $CH_4$ amounts agree to be near equilibrium. Also CO is formed and its concentration is also near equilibrium. By further decreasing temperature to 623 K, $CO_2$ conversion further increases, as methane yield does, while CO production is near to zero. However, we are now far than thermodynamic equilibrium, showing that kinetics governs the system at this lower temperature. This is true, even more, at 573 K and 523 K, where catalytic activity progressively tends to vanish. In spite of this, still methane is formed at 523 K with a 11 % yield. Thus, the “conditioned” catalyst is still active at 523 K.

In Fig. 2 the conversion obtained in the same conditions over $Ni/Al_2O_3$ catalyst are also reported. The results are also compared in Table 1 with each other and with the results of thermodynamic calculations. The performances of $Ni/Al_2O_3$ at 773 K are essentially the same as with $Ru/Al_2O_3$ and also correspond to equilibrium conditions. Instead at 673 K the conversion obtained on $Ni/Al_2O_3$ is clearly lower than that observed on “conditioned” $Ru/Al_2O_3$, confirming that the latter catalyst is more active than Ni-based one. In contrast to what happens with the $Ru/Al_2O_3$, the $Ni/Al_2O_3$ catalyst appears to be easily “conditioned” (the activity is stable after 10 min also at lower temperature, and appears to be stable during the run: in fact the performances of the catalyst at 523 K and 573 K in the decreasing temperature experiment are similar to those observed in the increasing temperature experiments. The maximum methane yield is obtained on $Ni/Al_2O_3$ at 673 K together with small amounts of CO. At lower temperatures the catalyst is fully selective to methane but it is less performant than $Ru/Al_2O_3$ in terms of methane yield.

To test the “conditioning” behavior of the $Ru/Al_2O_3$ catalyst, we performed runs after pre-reduction in $H_2/N_2$ at 673 K. The comparison of the data obtained after prereduction and without prereduction can be done by comparing the results reported in Table 1 and 2. It is evident that the prereduced catalyst is slightly more active than the non prereduced one in the starting experiments at low temperature, but still presents a “conditioning” step at 623 and 648 K, becoming then as active as the “fresh conditioned” catalyst. In the decreasing temperature steps the prereduced and non-prereduced catalysts behave in the same way, having been both “conditioned” in the previous high-temperature steps. TPR studies performed on $Ru/Al_2O_3$ catalysts indicate that Ru species should be reduced in hydrogen well below 573 K [23] although a very small amount of ruthenium is reported to need more than 973 K to be reduced [24]. The different behavior of prereduced and conditioned

catalysts suggest that conditioning may not only imply reduction but also some additional chemical conversion.

In Fig. 3, top the methane yield curve obtained on $Ru/Al_2O_3$ as a function of time on stream at 648 K is reported. The first two steps have been carried out at 298 K and at 573 K on the fresh catalyst. The activity is zero in the first step and very near zero in the second one. Then, the temperature was rapidly increased and set at 648 K. The conditioning effect on stream, that results in a progressive increase in $CO_2$ conversion and methane yield, is well evident. CO production is near zero in the entire experiment. Nearly 100 min are needed to stabilize conversion and yield to methane. A similar activation effect, limited to brief time, was reported to occur upon $CO_2$ methanation on preoxidized Rh ribbon [25]. We may mention here that conversion and yields are, at this temperature, governed by kinetics, being still not at thermodynamic equilibrium values ($X_{CO2}$=0.94; $Y_{CH4}$=0.939; $y_{CH4\ drygas}$=0.0728). The curve is successfully fitted by the equation:

$$y_{CH4} = 0.06718 - 0.07084 * e^{(-0.0562*t)} \quad (7)$$

where $y_{CH4}$ is the methane molar fraction (dry gas) in the effluent and t is time expressed in minutes.

The same experiment was done with Ni catalyst and reported in Fig. 3, bottom. In this case catalyst activation is essentially immediate with a constant co-production of CO with $CH_4$. At this temperature the catalyst is definitely less active as a methanation catalyst and also less selective than $Ru/Al_2O_3$.

In Fig. 4 the conversion of $CO_2$ and the yield to methane over the fresh $Ru/Al_2O_3$ catalyst are reported as a function of temperature and of space velocity. In the increasing temperature experiments, the catalyst is still under conditioning, and the catalytic activity is apparently poorly dependent on space velocity at low temperature. Instead, at high temperature, thermodynamic equilibrium is approached. In the decreasing temperature experiments, conversion lowers and yields decrease with respect to the thermodynamic values, confirming that the reaction enters in a kinetically controlled regime. Here the reaction rate dependence on space velocity is linear, as shown in Fig. 5, confirming that the regime is controlled by chemical kinetics, without relevant effects of diffusion phenomena. The linear dependence of conversion on contact time may be interpreted as an indication of the linear dependence of reaction rate on the number of active sites on the catalyst.

In Fig. 6 results of experiments performed over the fresh $Ru/Al_2O_3$ catalyst with different $CO_2$ concentrations are reported. The data show that, when the catalyst is conditioned (decreasing temperature experiments), the higher the $CO_2$ starting concentration, the higher the conversion. By increasing the reaction temperature the thermodynamic equilibrium is approached in all cases. At 573 and 523 K, instead, the system becomes under kinetic control.

The results coming from experiments performed at very small $CO_2$ conversion, when the differential reactor hypothesis can be valid, are reported in Fig. 7 for $Ni/Al_2O_3$ and $Ru/Al_2O_3$ catalysts, allowing thus to evaluate the reaction orders for $CO_2$ and $H_2$. In the upper diagrams, the dependence of methane yield on partial pressure of $CO_2$ are reported in conditions where $CO_2$ is the limiting reactant. In the lower diagrams, the dependence of methane yield on partial pressure of $H_2$ are reported in conditions where $H_2$ is the limiting reactant.

In the case of $Ru/Al_2O_3$ catalyst, the kinetic order with respect to $CO_2$ concentration is zero, while the kinetic order with respect to $H_2$ is 0.39. These data substantially agree with some previous results [26]. On $Ni/Al_2O_3$ a slightly positive $CO_2$ reaction order is found, in 0.17, while the $H_2$ reaction order is 0.32, also similar to previously published data [27], and slightly lower than that found on $Ru/Al_2O_3$. The activation energies evaluated in this the temperature range 493-573 K are 60 kJ/mol and 80 kJ/mol approx. for $Ru/Al_2O_3$ and $Ni/Al_2O_3$ catalysts, respectively, confirming that we are working in a chemical kinetic regime.

As shown above, the $Ru/Al_2O_3$ catalyst may need a pretreatment or a conditioning time on stream to rise optimal activity. To test its applicability in cyclic or intermittent conditions, the same catalytic bed was used several times with different shut-down and start-up procedures, as shown in Fig. 8. The catalyst quickly provided the same performances independent on the procedures adopted. A difference may be appreciated looking at carbon dioxide conversion ($X_{CO2}$) at 523 K that passes from 11% (as reported in table one) to the maximum value of 26% in the last cycle) thus increasing even its activity after cycles.

The obtained data allow us to treat the catalyst conditioning phenomenon in a similar way to that used for catalyst deactivation phenomenon [28] and in parallel with the procedure proposed by Wilkinson et al. [29]. The data provided in the first cycle at 648 K (Fig. 3, top) allow us to propose the following experimental expression for reaction kinetics in kinetically limited conditions when $CO_2$ conversion only produces methane:

$r_{CH4} = - r_{CO2} = (-dP_{CO2}/dt) = dP_{CH4}/dt = k\, e^{(-E_A/RT)}\, P_{CO2}^{0}\, P_{H2}^{0.39}\, n_{SA}$ (8)

where $n_{SA}$ is the number of the active sites for the reaction.

A similar expression can be used to model the dependence of reaction rate on time on stream during the conditioning period at constant temperature.

$r_{CH4}(t) = d(P_{CH4}(t))/dt = k' P_{CO2}^{0} P_{H2}^{0.39} a(t)$ (9)

where the activity a(t) is defined as follows:

$a(t) = A\, n_{SA}(t) = r_{CH4}(t)/ r_{CH4\,(ss)}$ (10)

where $r_{CH4\,(ss)}$ is the reaction rate at steady state. In this approach the activity is assumed to depend linearly on the number of the active sites as shown above for the reaction rate.

Thus, the rate of activity evolution da/dt is

$da/dt = Q(T,C)\,(1-a)^{n}$ (11)

where Q(T,C) is the “constant of activity evolution” [29].

By integrating this equation it follows that, only assuming n=1

$a(t) = 1 - \exp(-Qt)$ (12)

This expression is equivalent to the expression (7) as an effect of normalization (10).

Thus the value Q(T,C)=0.0583 represents the numerical value of the conditioning kinetic constant. The characteristic conditioning time could be expressed as $t_A = 1/Q$

In Figure 9 FE-SEM and EDX analyses of the fresh $Ru/Al_2O_3$ catalyst are reported. In the case of the fresh catalyst, FE-SEM micrograph shows essentially well dispersed Ru species on alumina, since particles brightness appears quite homogeneous in the micrograph collected with the backscattered electrons detector (BSE). However few small particles with strong brightness are present showing that part of ruthenium agglomerated in Ru rich particles. Interestingly the EDX analysis recorded on the particle shows together with the expected presence of Ru, Al and O non negligible amount of chlorine (the detection of carbon and copper is not relevant because they are contained in the sample holder).

The FE-SEM analysis of the conditioned $Ru/Al_2O_3$ (Figure 10) catalyst reveals a partial agglomeration of ruthenium, being now more evident areas of stronger brightness. On the other hand, simultaneously recorded EDX analysis shows no more chlorine. This result can provide some additional insights on the conditioning mechanism of the catalyst. It seems likely that the activity of the catalyst simply reduced in $H_2$ is hindered by the presence of chlorine. The conditioning on stream may be associated to the huge amount of water produced during methanation that likely allows the elimination of chlorine from the surface producing gaseous HCl.

Analogous FE-SEM/EDX experiments have been performed with $Ni/Al_2O_3$ catalyst and are reported in Figs. 11 and 12. According to the higher loading, in this case, metal rich particles are evident both in the fresh (Fig. 11) and in the used catalysts (Fig.12) but the agglomeration of Nickel is evident after reaction. In fact Ni rich particles increase in size from about ten nanometers to several tens of nanometers.
The situation is similar to that already described for home-made Ni alumina catalysts [15] even if a better dispersion of Nickel was obtained in that case.

## 4. Conclusions.

The data reported here confirm that 3% $Ru/Al_2O_3$ is an excellent catalyst for $CO_2$ methanation. In our reaction conditions, 96 % yield to methane can be obtained with no CO coproduction at 573 K at 30000 $h^{-1}$ GHSV in excess hydrogen, in spite of the low partial pressures conditions. The performance is better than that of a 20% $Ni/Al_2O_3$ catalyst where maximum yields approach 80 % at 673 K, with some CO coproduction.

Over the 3% $Ru/Al_2O_3$ catalyst the kinetic reaction orders where measured to be zero for $CO_2$ and slightly positive (0.39) for hydrogen. These reaction orders suggest that both $CO_2$ and hydrogen are strongly adsorbed on the surface, thus giving rise to a Langmuir–Hinshelwood type reaction mechanism. The $CO_2$ reaction order observed on $Ni/Al_2O_3$ catalyst is slightly higher, although it may be considered that it has been measured at a slightly higher temperature. Over both catalysts the hydrogen reaction order is in the range 0.3-0.4.

Our study shows that, to provide optimal activity, the $Ru/Al_2O_3$ catalyst must be conditioned on stream, simple reduction in hydrogen not giving rise to a fully active catalyst. This behaviour suggests that activation implies not only reduction but also other chemical conversion. Indeed, FE-SEM/EDX study show that conditioning results in disappearance of chlorine which likely poisons the fresh and reduced catalyst. Additional conditioning results also in some agglomeration of ruthenium. In contrast the $Ni/Al_2O_3$ is rapidly activated in hydrogen. On the other hand, conditioned $Ru/Al_2O_3$ catalyst appears to be highly stable also after different shut-down and start-up procedures, thus being likely applicable in intermittent conditions.

Acknowledgements

The collaboration of Giulia Pastorino in performing a part of the catalytic experiments is gratefully acknowledged.

TABLES

Table 1: $CO_2$ conversion ($X_{CO2}$) , methane and CO yields ($Y_{CH4}$, $Y_{CO}$) on as prepared 3%$Ru/Al_2O_3$ GHSV=55000 $h^{-1}$, 20%$Ni/Al_2O_3$ and according to thermodynamic equilibrium.

| | 3%$Ru/Al_2O_3$ as prepared | | | 20%$Ni/Al_2O_3$ as prepared | | | Thermodynamic Equilibrium | | |
|---|---|---|---|---|---|---|---|---|---|
| T [K] | X $CO_2$ | Y $CH_4$ | Y CO | X $CO_2$ | Y $CH_4$ | Y CO | X $CO_2$ | Y $CH_4$ | Y CO |
| 523 | 3% | 3% | 0% | 4% | 4% | 0% | 99,99% | 99,99% | 0,00% |
| 573 | 4% | 4% | 0% | 20% | 20% | 0% | 99,80% | 99,80% | 0,00% |
| 623 | 23%→39% | 23%→39% | 0% | 58% | 54% | 4% | 97,39% | 97,31% | 0,08% |
| 673 | 72%→79% | 69%→77% | 3% | 77% | 73% | 4% | 89,89% | 89,17% | 0,72% |
| 723 | 76% | 69% | 7% | 79% | 72% | 7% | 79,84% | 76,32% | 3,52% |
| 773 | 69% | 55% | 15% | 74% | 62% | 12% | 71,27% | 59,58% | 11,69% |
| 723 | 76% | 68% | 8% | 79% | 76% | 4% | 79,84% | 76,32% | 3,52% |
| 673 | 85% | 82% | 3% | 81% | 78% | 2% | 89,89% | 89,17% | 0,72% |
| 623 | 86% | 86% | 0% | 59% | 59% | 0% | 97,39% | 97,31% | 0,08% |
| 573 | 59% | 59% | 0% | 21% | 21% | 0% | 99,80% | 99,80% | 0,00% |
| 523 | 11% | 11% | 0% | 4% | 4% | 0% | 99,99% | 99,99% | 0,00% |

Table 2: $CO_2$ conversion ($X_{CO2}$), methane and CO yields ($Y_{CH4}$, $Y_{CO}$) on prereduced 3%$Ru/Al_2O_3$ GHSV=55000 $h^{-1}$

| T [K] | X $CO_2$ | Y $CH_4$ | Y CO |
|---|---|---|---|
| 523 | 2% | 2% | 0% |
| 573 | 10% | 10% | 0% |
| 623 | 30% | 30% | 0% |
| 623 | 39% | 39% | 0% |
| 623 | 43% | 43% | 0% |
| 648 | 65% | 62% | 3% |
| 648 | 70% | 67% | 3% |
| 648 | 74% | 70% | 3% |
| 673 | 81% | 76% | 5% |
| 673 | 82% | 77% | 5% |
| 673 | 83% | 78% | 5% |
| 723 | 77% | 66% | 11% |
| 773 | 71% | 48% | 23% |
| 773 | 71% | 53% | 18% |
| 723 | 77% | 69% | 9% |
| 673 | 87% | 84% | 3% |
| 648 | 91% | 91% | 0% |
| 623 | 93% | 93% | 0% |
| 573 | 66% | 66% | 0% |
| 523 | 22% | 22% | 0% |

Figure captions

Figure 1: $CO_2$, CO and $CH_4$ absorbances in function of time during the increasing and decreasing Temperature experiment on 3%$Ru/Al_2O_3$ catalyst in the following conditions: 6%$CO_2$, 30% $H_2$, 64% $N_2$, 75 Nml/min with a GHSV= 55000 $h^{-1}$

Figure 2: $CO_2$, CO and $CH_4$ absorbances in function of time during the increasing and decreasing Temperature experiment on 20%$Ni/Al_2O_3$ catalyst in the following conditions: 6%$CO_2$, 30% $H_2$, 64% $N_2$, 75 Nml/min with a GHSV= 55000 $h^{-1}$

Figure 3: $CO_2$, CO and $CH_4$ absorbances in function of time at RT, at 523 K and 648 K for 3%$Ru/Al_2O_3$ catalyst (top) and 20%$Ni/Al_2O_3$ catalyst (bottom) in the following conditions: 6%$CO_2$, 30% $H_2$, 64% $N_2$, 75 Nml/min with a GHSV= 55000 $h^{-1}$

Figure 4: Experimental $CO_2$ conversion and $CH_4$ yield as a function of Temperature and GHSV together with the displacement of the thermodynamic equilibrium

Figure 5: $CO_2$ conversion in function of the contact time (calculated as volume of catalyst on total flowrate (NTP)) and linear fit

Figure 6: Experimental (E) $CO_2$ conversion and $CH_4$ yield as a function of Temperature and $CO_2$ concentration together with the displacement of the thermodynamic equilibrium (T)

Figure 7: Methane production rate as a function of $p_{CO2}$ for 3%$Ru/Al_2O_3$ and 20%$Ni/Al_2O_3$ (top) and as a function of hydrogen partial pressure ($p_{H2}$) (bottom), with determination of the reaction orders

Figure 8: $CO_2$, CO and $CH_4$ absorbances in function of time at RT, at 523 K and 648 K for 3%$Ru/Al_2O_3$, during intermittent operations in cyclic conditions (cycles 2, 5 and 9).

Figure 9: FE-SEM micrographs of fresh 3%$Ru/Al_2O_3$ showing catalyst morphology as recorded with InLens detector (top). In the inset, the micrograph recorded using the backscattered electrons (BSE). Bottom: EDX analysis recorded on an area of the particle

Figure 10: FE-SEM micrographs of conditioned 3%$Ru/Al_2O_3$ showing catalyst morphology as recorded with InLens detector (top, left) and with backscattered electron (top right). In the inset, the micrograph recorded using the backscattered electrons (BSE). Bottom: EDX analysis recorded on an area of the sample.

Figure 11: FE-SEM micrographs of fresh 20%$Ni/Al_2O_3$ showing catalyst morphology as recorded with InLens detector (top, left) and with backscattered electron (top right). In the inset, the micrograph recorded using the backscattered electrons (BSE). Bottom: EDX analysis recorded on an area of the sample.

Figure 12: FE-SEM micrographs of used 20%$Ni/Al_2O_3$ showing catalyst morphology as recorded with InLens detector (top, left) and with backscattered electron (top right). In the inset, the micrograph recorded using the backscattered electrons (BSE). Bottom: EDX analysis recorded on an area of the sample.

References


[1] Wender I, Reactions of synthesis gas. Fuel Proc Technol 1996; 48:189.

[2] Twigg MV, Catalyst Handbook, 2nd ed., 1989, pp. 283-339.

[3] http://www.jmcatalysts.com/ptd/pdfs-uploaded/Delivering%20world%20class%20ammonia%20plant%20performance.pdf

[4] http://www.topsoe.com/business_areas/ammonia/~/media/PDF%20files/Methanol/Topsoe_methanation_pk_7r.ashx

[5] http://www.catalysts.clariant.com/bu/Catalysis/internet.nsf/023cfbb98594ad5bc12564e400555162/4cf78747d693c1f0c1257ad0002d2c04?OpenDocument

[6] Rase HF, Handbook of Commercial Catalysts: Heterogeneous Catalysts, Boca Raton, CRC press, 2000, p.447.

[7] http://www.topsoe.com/products/pk-7r

[8] Hoekman SK, Broch A, Robbins C, Purcell R, Int J Green Gas Control 2010;4:44–50

[9] Kopyscinski J, Schildhauer T J, Biollaz SMA, Production of synthetic natural gas (SNG) from coal and dry biomass - A technology review from 1950 to 2009. Fuel 2010; 89:1763–83

[10] Nguyen TTM, Wissing L, Skjøth-Rasmussen MS, High temperature methanation: Catalyst considerations. Catal Today 2013;215:233–8

[11] http://www.topsoe.com/products/CatalystPortfolio.aspx

[12] Røstrup-Nielsen JR, Pedersen K, Sehested J, High temperature methanation. Sintering and structure sensitivity, Appl. Catal. A: Gen. 2007;330:134-8.

[13] Wang W, Gong J, Methanation of Carbon Dioxide: An Overview, Front. Chem. Sci. Eng. 2011;5:2-10

[14] Abelló S, Berrueco C, Montané D, High-loaded nickel–alumina catalyst for direct $CO_2$ hydrogenation into synthetic natural gas (SNG) Fuel 2013;113:598–609

[15] Garbarino G, Riani P, Magistri L, Busca G, A study of the methanation of carbon dioxide on $Ni/Al_2O_3$ catalysts at atmospheric pressure Int J Hydr En 2014;39:11557-565

[16] Scholten SA, Alhson JD, Dunn BC, Methanation Reaction Methods Utilizing Enhanced Catalyst Formulations and Methods of Preparing Enhanced Methanation Catalysts, patent application n. US 20120238647 A1, to Conocophillips Co. 2012

[17] Karelovic A, Ruiz P, $CO_2$ hydrogenation at low temperature over $Rh/\gamma\text{-}Al_2O_3$ catalysts: Effect of the metal particle size on catalytic performances and reaction mechanism, Appl. Catal. B: Environ., 2012;113-114:237-49

[18] Kwak JH, Kovarik L, Szanyi L, $CO_2$ Reduction on Supported $Ru/Al_2O_3$ Catalysts: Cluster Size Dependence of Product Selectivity, ACS Catal. 2013;3:2449-55

[19] Janke C, Duyar MS, Hoskins M, Farrauto R, Catalytic and adsorption studies for the hydrogenation of $CO_2$ to methane, Appl Catal B:Environ. 2014;152-3:184-91

[20] “Pearson Crystal Data: Crystal structure database for inorganic compounds” , Release 2009/2012, ASM International, The Material Information Society

[21] Fogler HS, Elements of Chemical Reaction Engineering, fourth ed., Pearson Education International, New Jersey, 2006.

[22] Reid RD, Prausnitz JM, Poling BE, The Properties of Gases and Liquids, 4th ed.; McGraw-Hill: New York, 1986.

[23] Betancourta P,. Rives A, Hubaut R, Scotta CE, Goldwasser J, A study of the ruthenium±alumina system, Appl Catal A: Gen 1998;170:307-14

[24] Wang M, Weng W, Zheng H, Yi X, Huang C, Wan H, J Nat Gas Chem 2009;18:300-5.

[25] Amariglio A, Lakhdar M, Amariglio H, Methanation of Carbon Dioxide over Preoxidized Rhodium, J Catal 1983;81:247-51

[26] Praire MR, Renken A, Highfield JG, Thampi KR, Grxtzel M, A Fourier Transform Infrared Spectroscopic Study of $CO_2$ Methanation on Supported Ruthenium, J Catal 1991;129:130-44

[27] Fujita S, Nakamura M, Doi T, Takezawa N, Mechanisms of methanation of carbon dioxide and carbon monoxide over nickel/alumina catalysts, Appl Catal A: Gen 1993;104:87–100

[28] Fuentes GA, Catalyst deactivation model and steady-state activity: a generalized power-law equation model, Appl Catal 1985;15:33-40

[29] Wilkinson SK, Simmonjs MJH, Stitt EH, Baucherel X, Watson MJ, A novel approach to understanding and modeling performance evolution of catalysts during their initial operation under reaction conditions- Case study of vanadium phosphorous oxides for n-butane selective oxidation, J Catal 2013;299:249-60

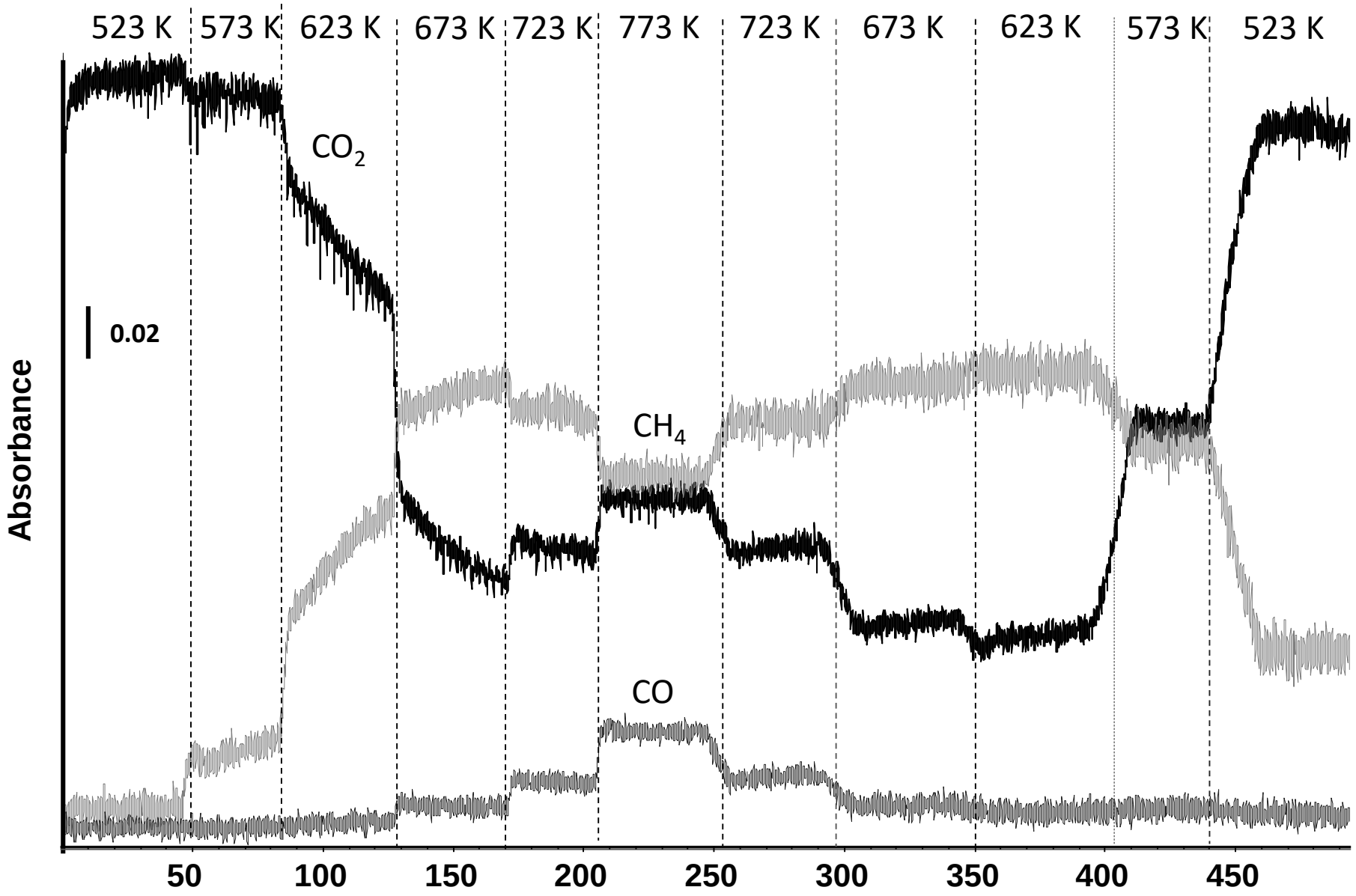
523 K
573 K
623 K
673 K
723 K
773 K
723 K
673 K
623 K
573 K
523 K
CO2
CH4
CO
0.02
Absorbance
50
100
150
200
250
300
350
400
450

Figure 1

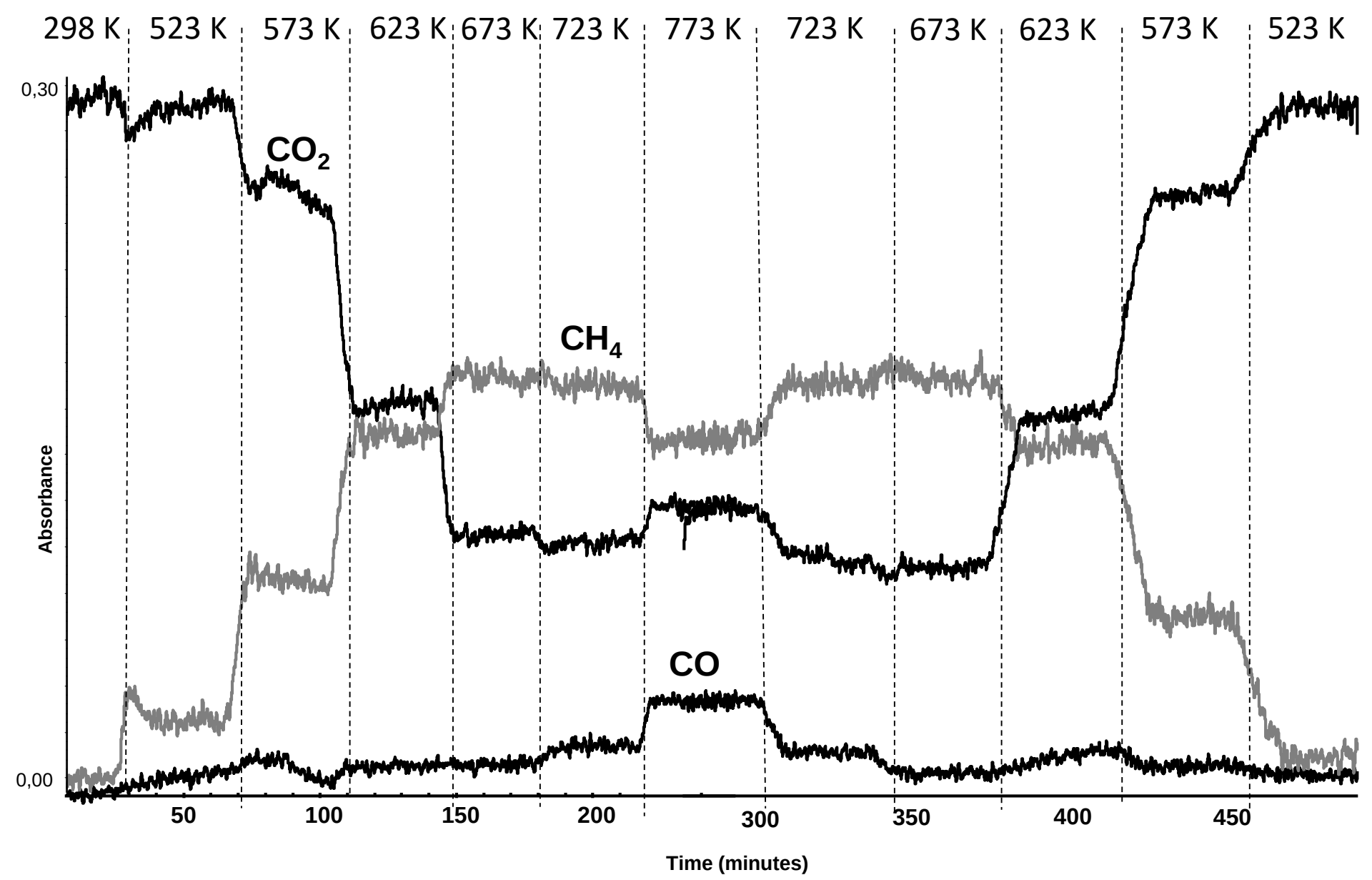
298 K
523 K
573 K
623 K
673 K
723 K
773 K
723 K
673 K
623 K
573 K
523 K
0,30
0,00
Absorbance
CO2
CH4
CO
50
100
150
200
300
350
400
450
Time (minutes)

Figure 2

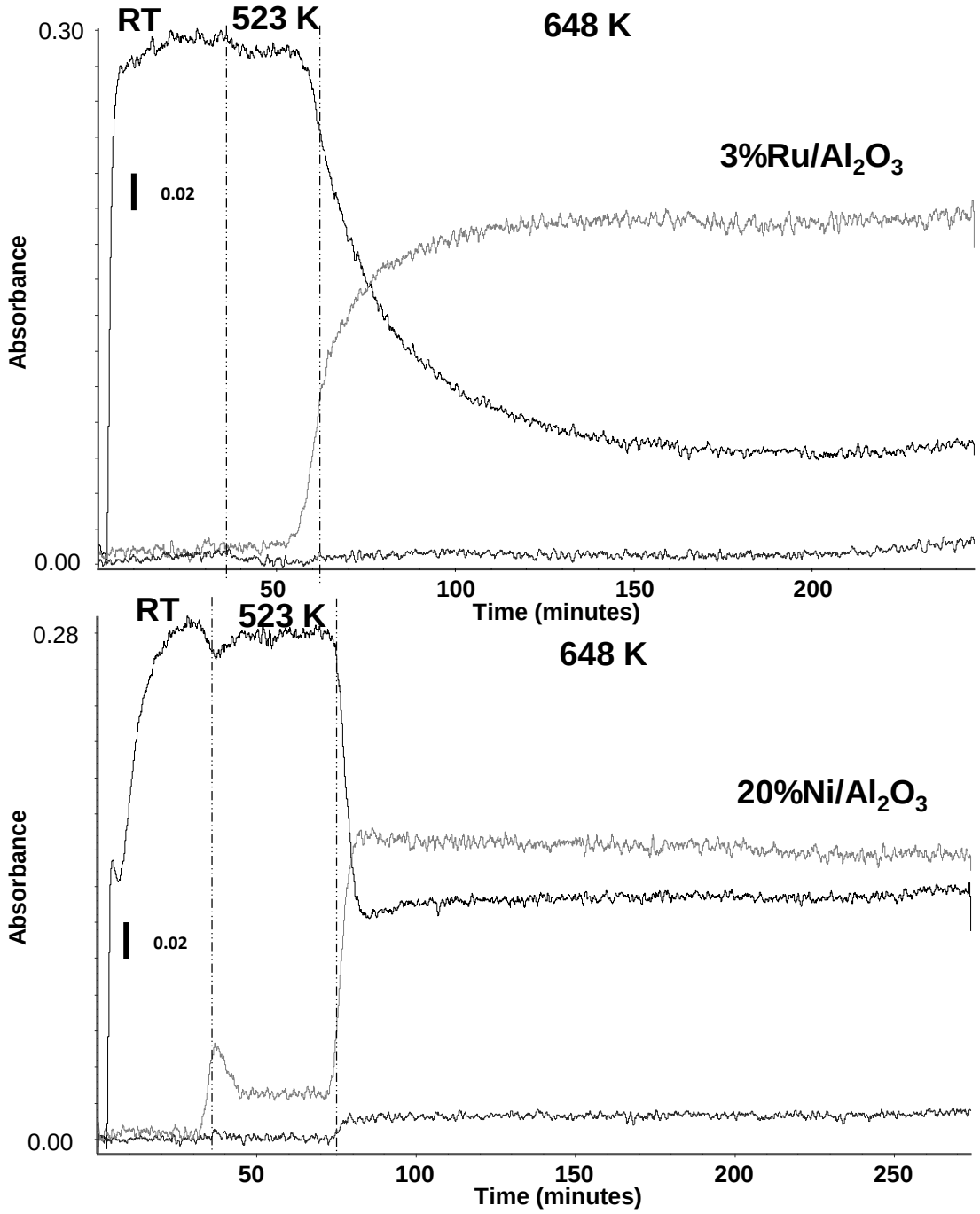
RT
523 K
648 K
0.30
0.00
Absorbance
0.02
3%Ru/Al2O3
50
100
150
200
Time (minutes)
RT
523 K
648 K
0.28
0.00
Absorbance
0.02
20%Ni/Al2O3
50
100
150
200
250
Time (minutes)

Figure 3

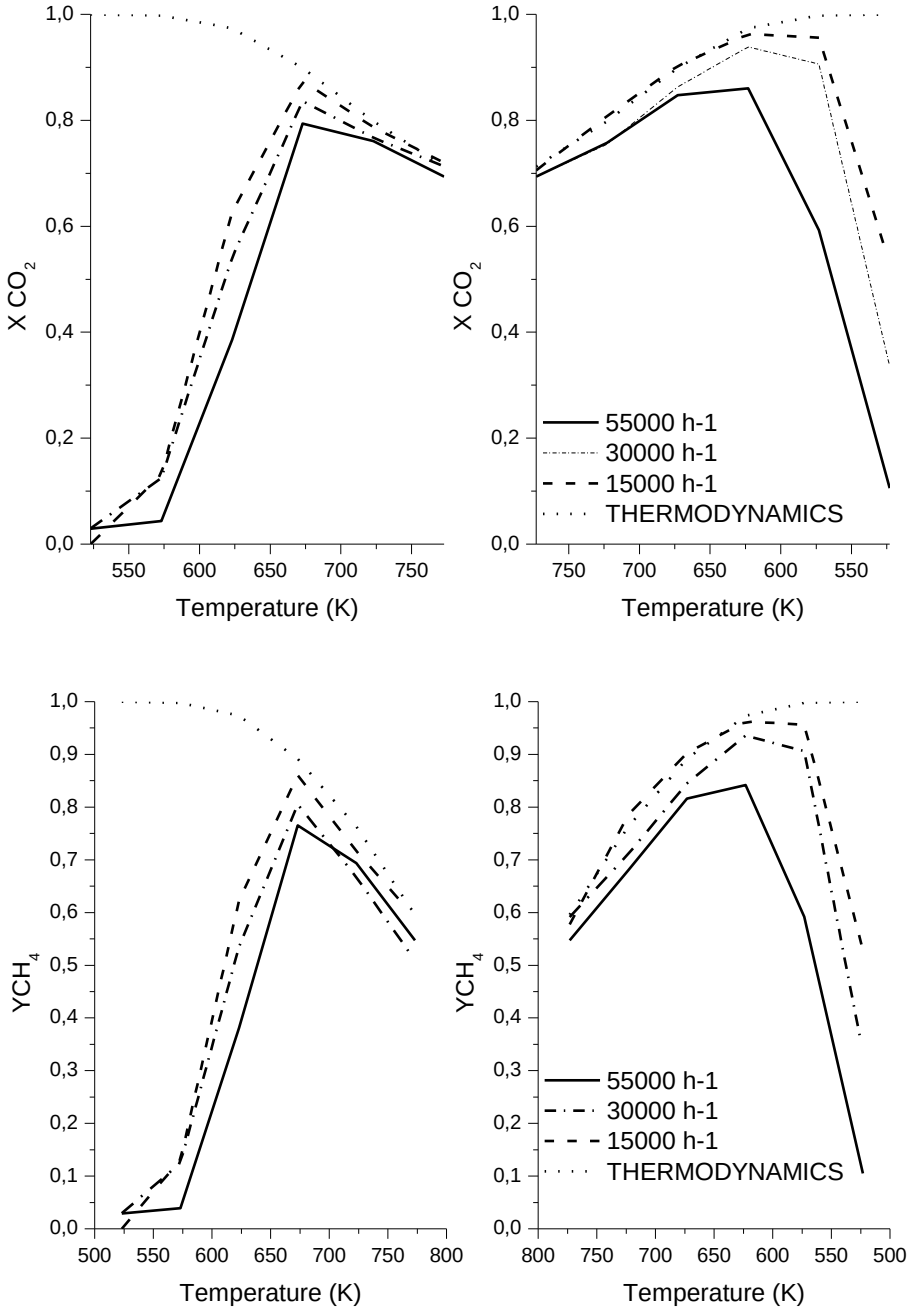
X CO2
Temperature (K)
55000 h-1
30000 h-1
15000 h-1
THERMODYNAMICS
YCH4
Temperature (K)

Figure 4

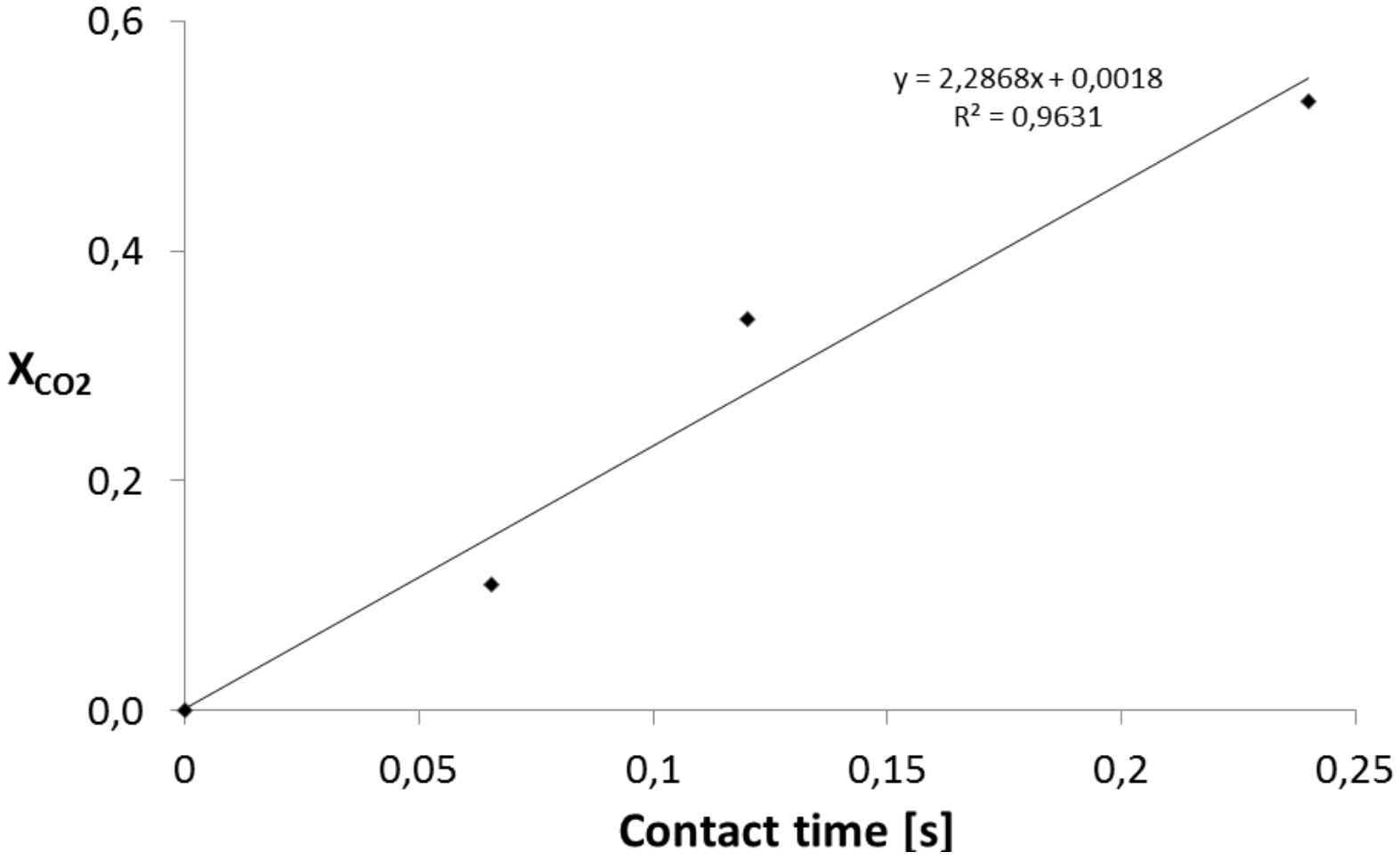
y = 2,2868x + 0,0018
R² = 0,9631
0,6
0,4
0,2
0,0
$X_{CO2}$
0
0,05
0,1
0,15
0,2
0,25
Contact time [s]

Figure 5

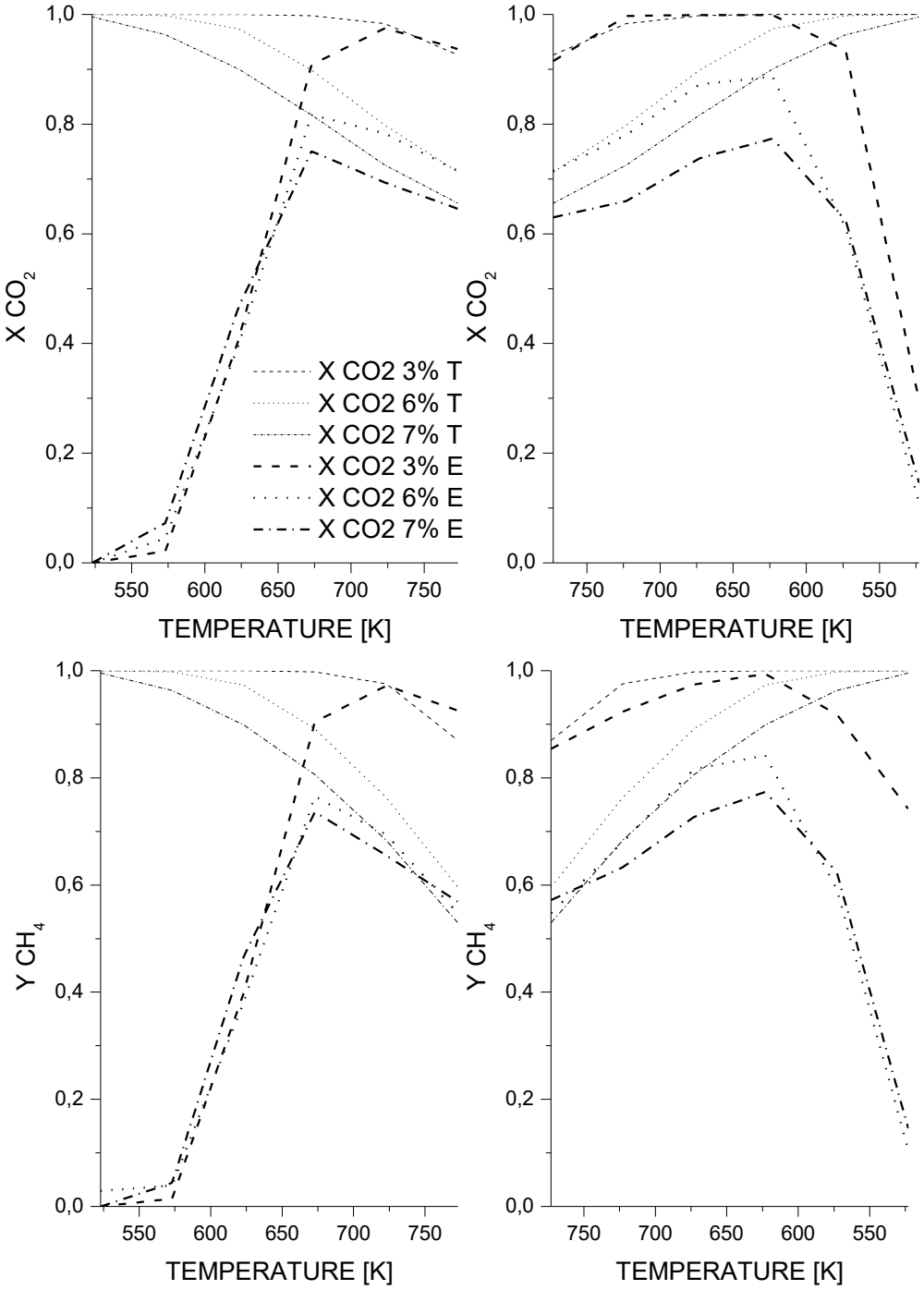
X CO2 3% T
X CO2 6% T
X CO2 7% T
X CO2 3% E
X CO2 6% E
X CO2 7% E
X CO2
Y CH4
TEMPERATURE [K]
1,0
0,8
0,6
0,4
0,2
0,0
550
600
650
700
750

Figure 6

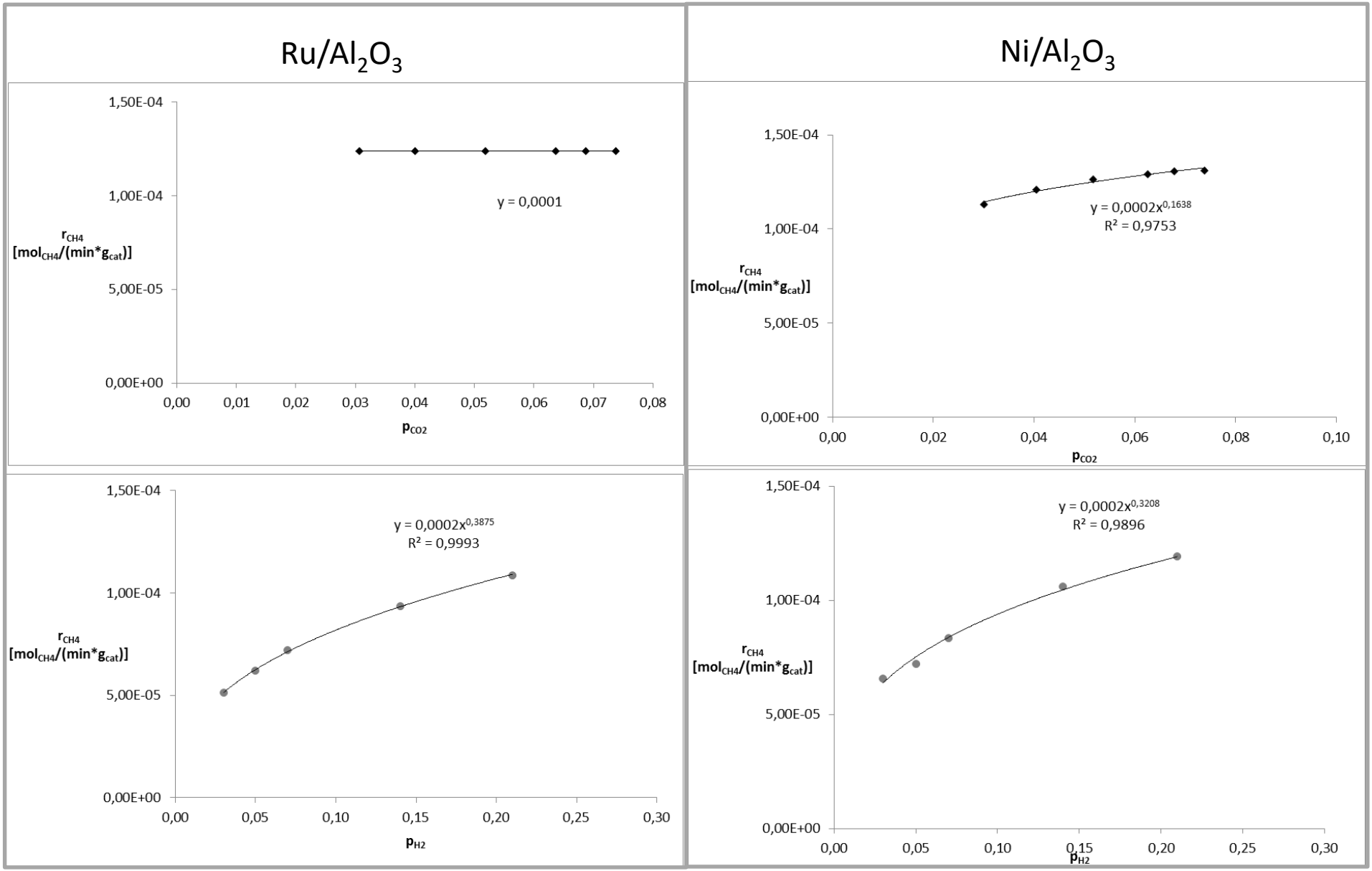
Ru/Al2O3
Ni/Al2O3
1,50E-04
1,00E-04
5,00E-05
0,00E+00
y = 0,0001
rCH4
[molCH4/(min*gcat)]
0,00 0,01 0,02 0,03 0,04 0,05 0,06 0,07 0,08
pCO2
y = 0,0002x0,1638
R² = 0,9753
0,00 0,02 0,04 0,06 0,08 0,10
y = 0,0002x0,3875
R² = 0,9993
0,00 0,05 0,10 0,15 0,20 0,25 0,30
pH2
y = 0,0002x0,3208
R² = 0,9896

Figure 7

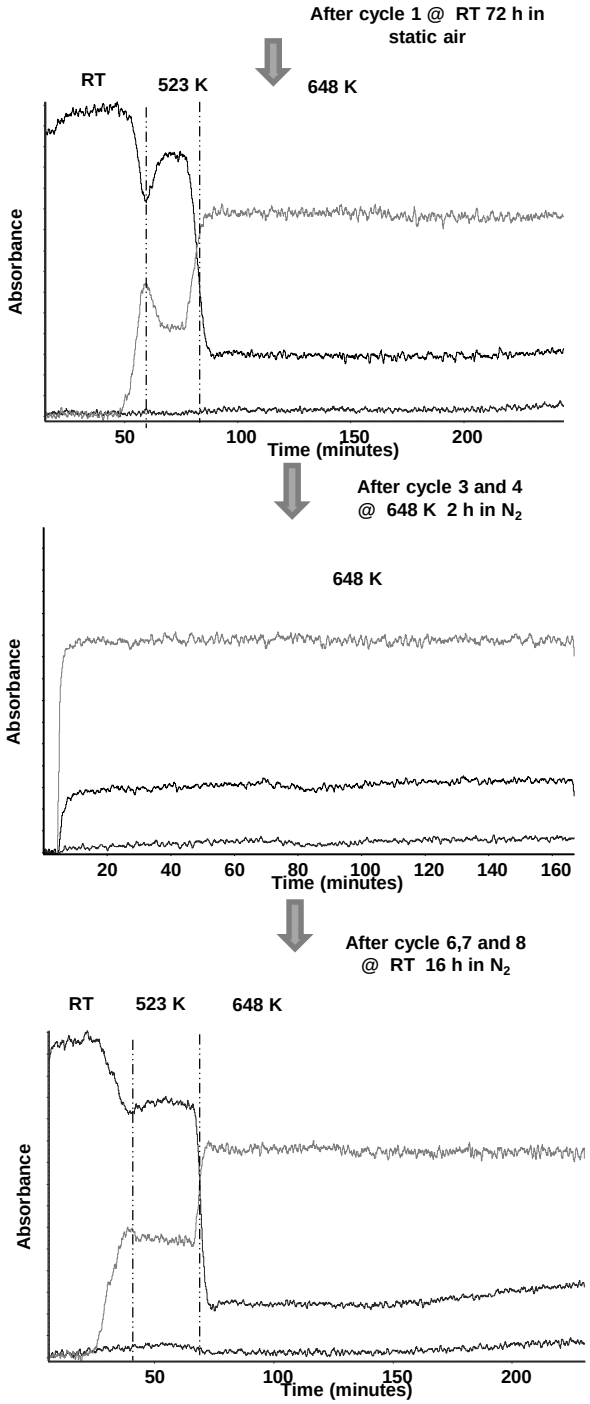
After cycle 1 @ RT 72 h in static air
RT
523 K
648 K
Absorbance
50
100
150
200
Time (minutes)
After cycle 3 and 4 @ 648 K 2 h in N2
648 K
Absorbance
20
40
60
80
100
120
140
160
Time (minutes)
After cycle 6,7 and 8 @ RT 16 h in N2
RT
523 K
648 K
Absorbance
50
100
150
200
Time (minutes)

Figure 8

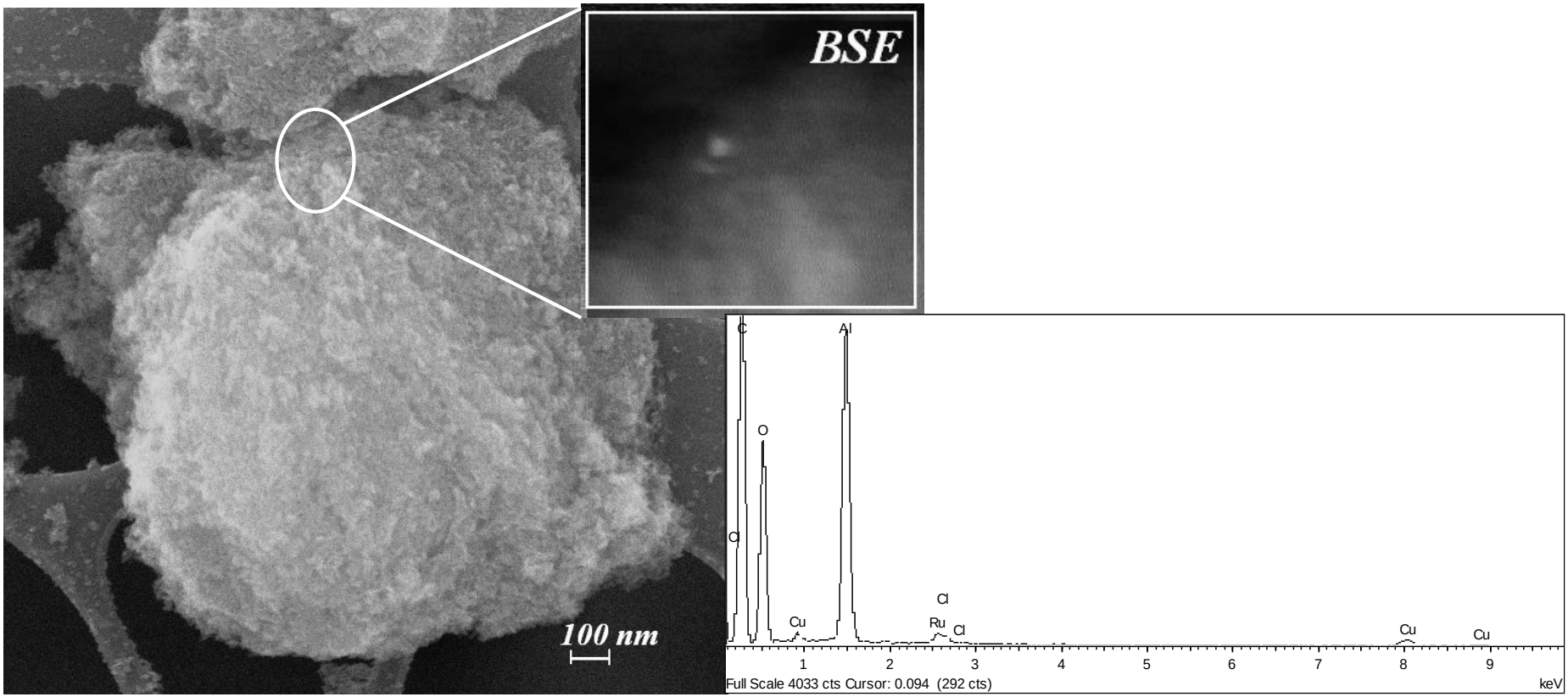
BSE
100 nm
C
Al
O
Cl
Cu
Ru
Cl
Cl
Cu
Cu
1
2
3
4
5
6
7
8
9
Full Scale 4033 cts Cursor: 0.094 (292 cts)
keV

Figure 9

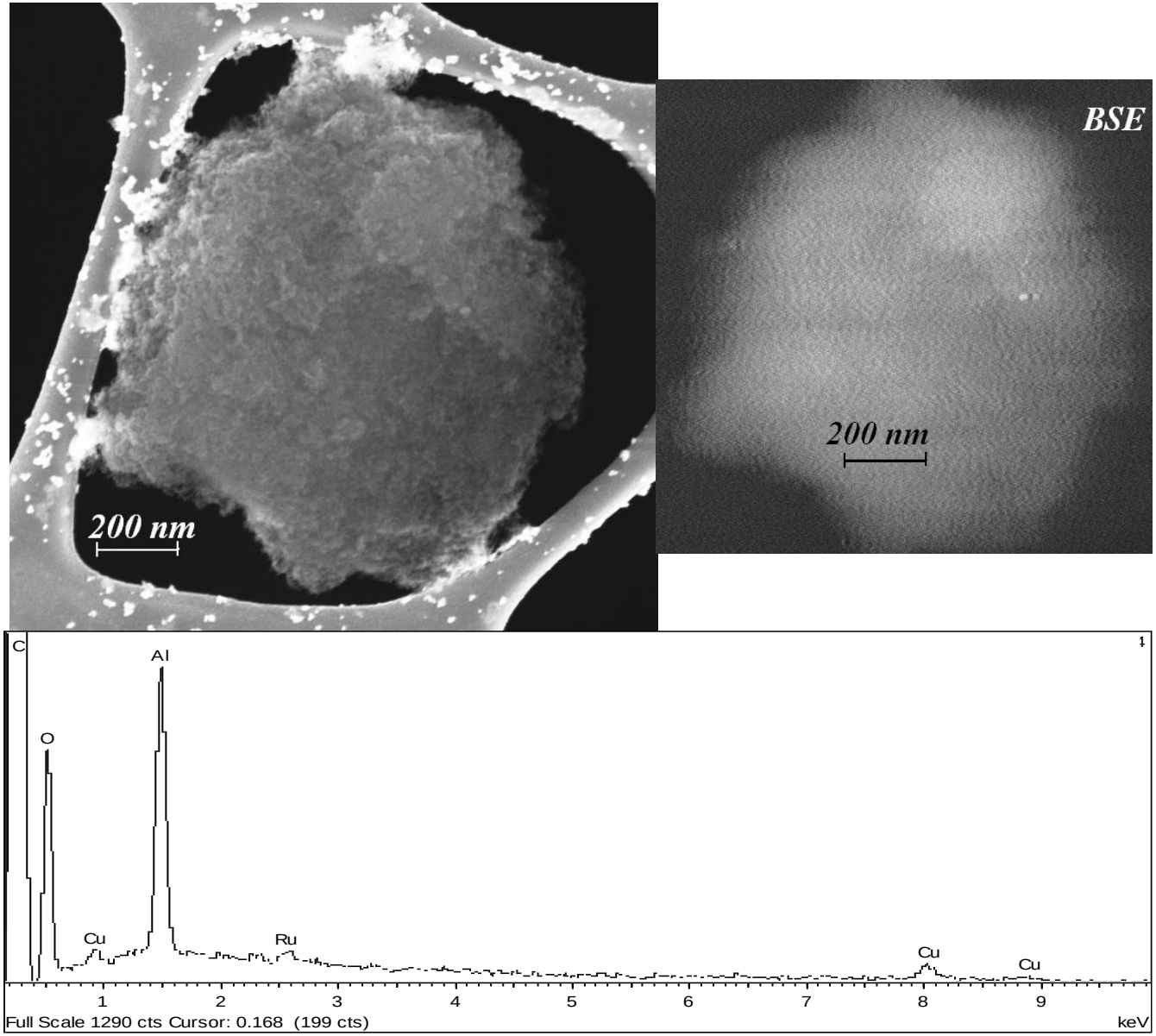
200 nm
BSE
200 nm
C
O
Al
Cu
Ru
Cu
Cu
1
2
3
4
5
6
7
8
9
Full Scale 1290 cts Cursor: 0.168 (199 cts)
keV

Figure 10

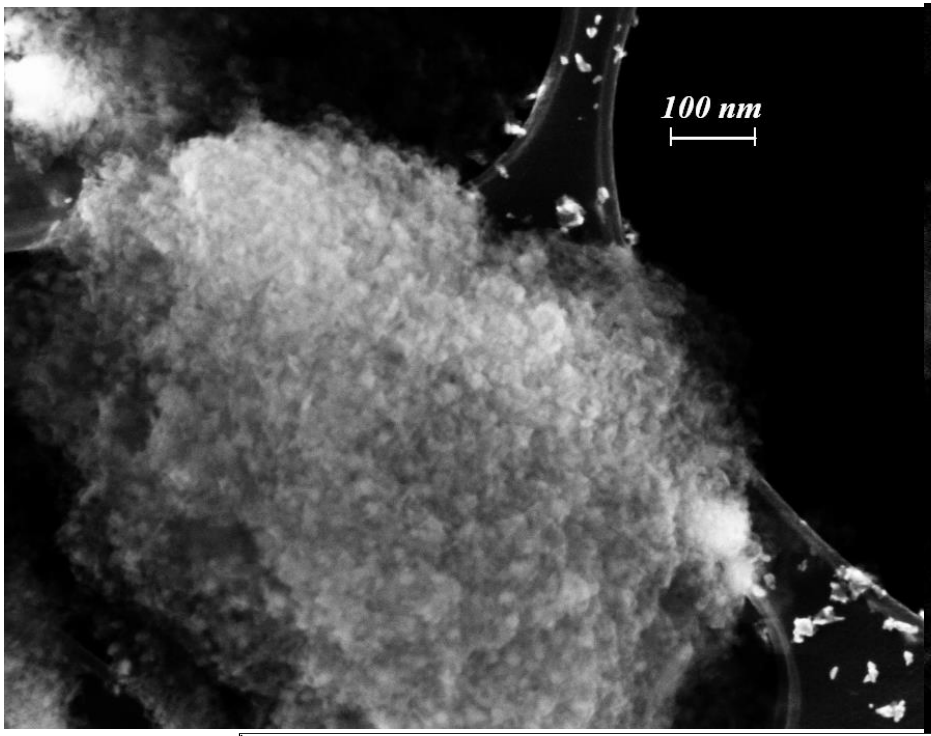
100 nm

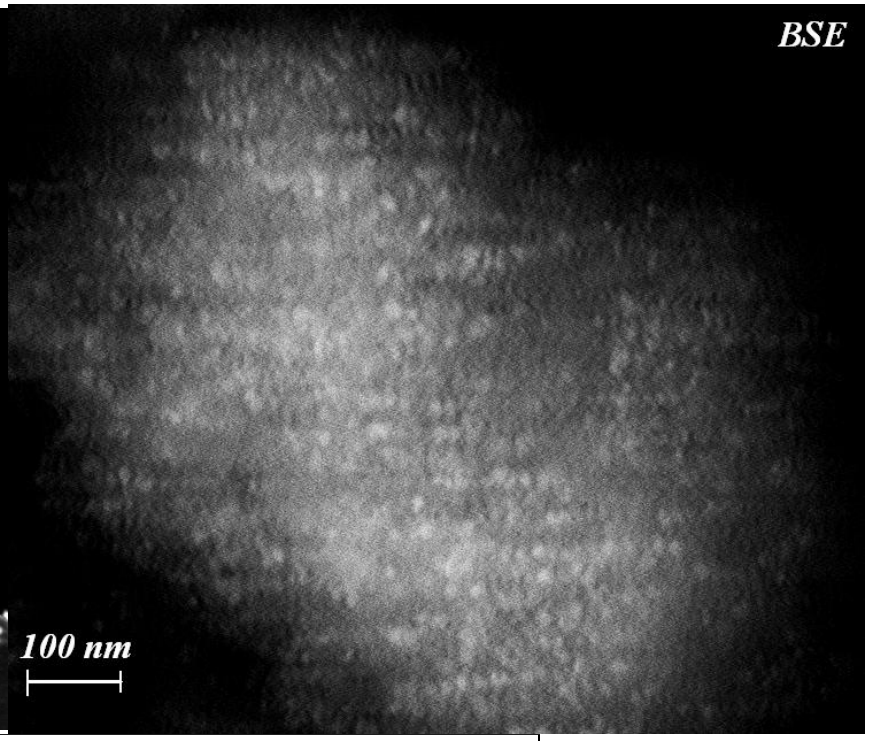
BSE
100 nm

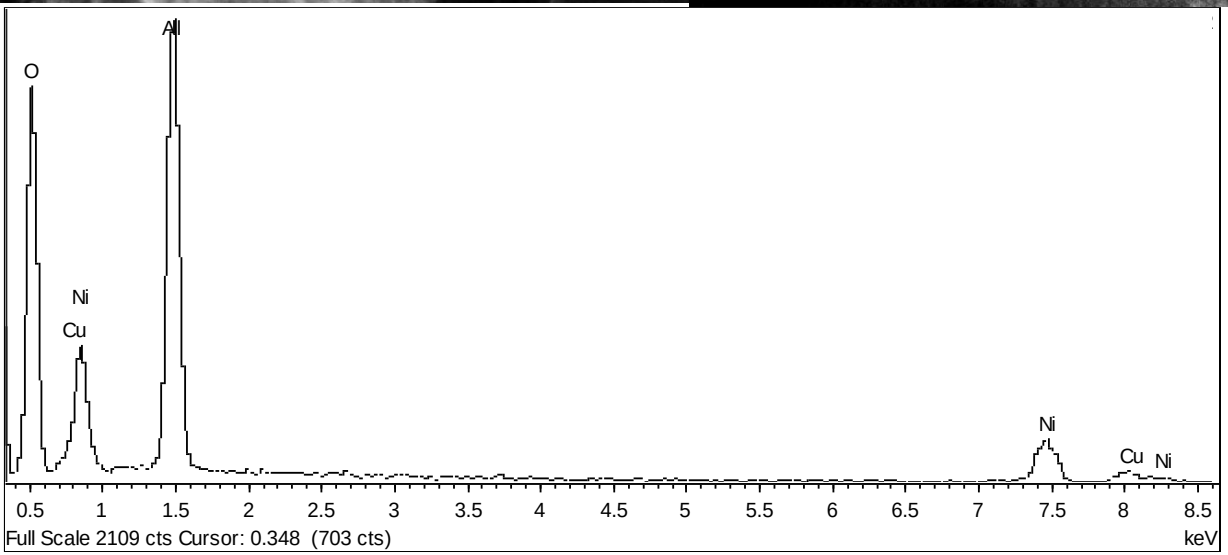
O
Al
Ni
Cu
Ni
Cu
Ni
0.5 1 1.5 2 2.5 3 3.5 4 4.5 5 5.5 6 6.5 7 7.5 8 8.5
Full Scale 2109 cts Cursor: 0.348 (703 cts)
keV

Figure 11

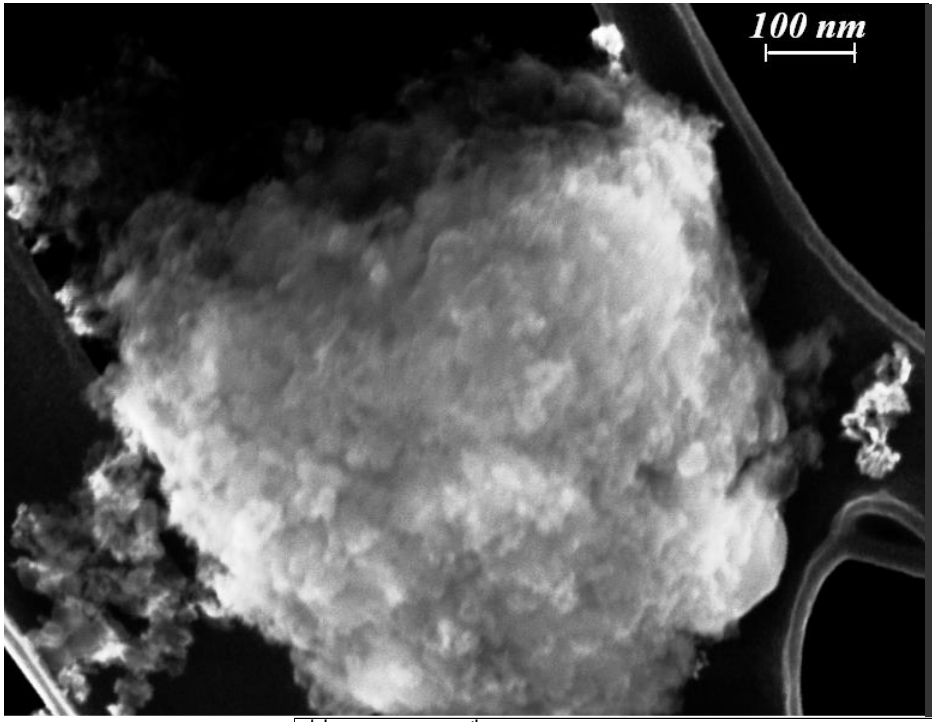
100 nm

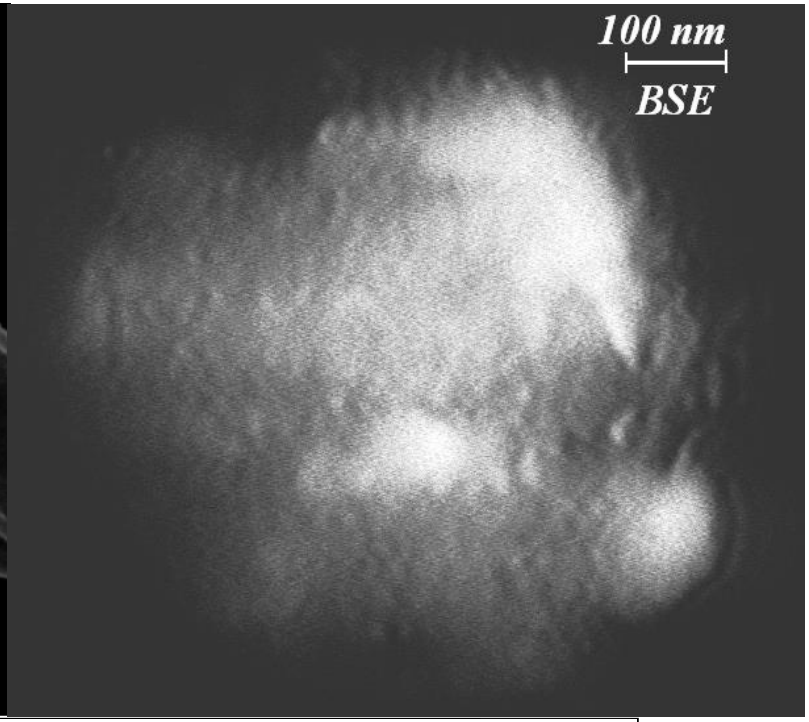
100 nm
BSE

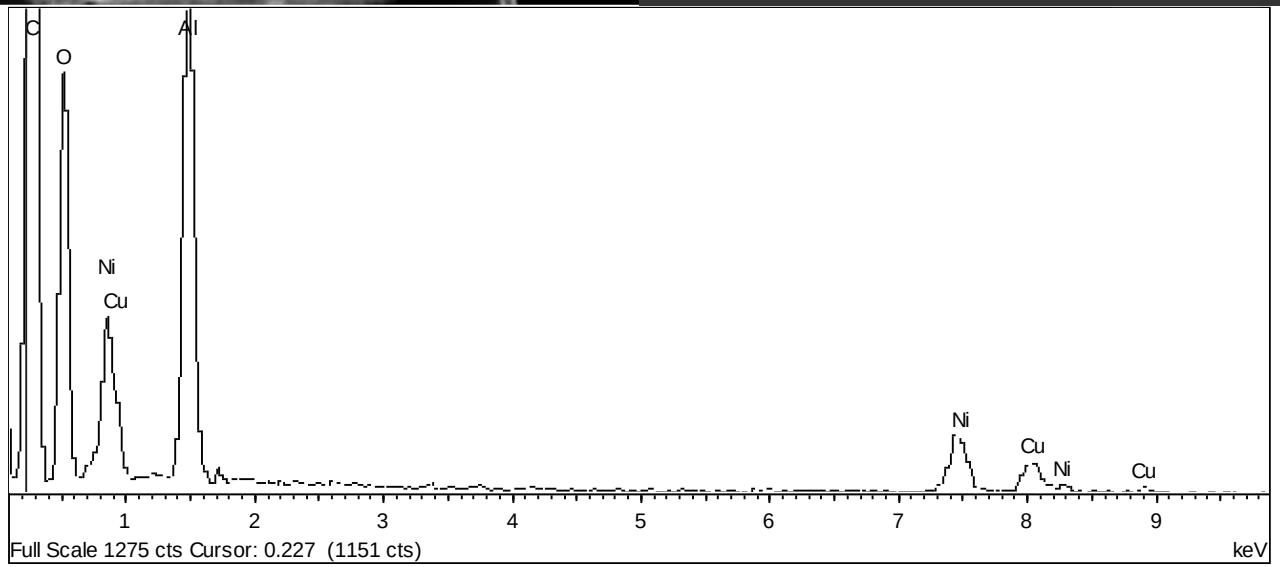
C
O
Al
Ni
Cu
Ni
Cu
Ni
Cu
1
2
3
4
5
6
7
8
9
Full Scale 1275 cts Cursor: 0.227 (1151 cts)
keV

Figure 12